Effects of Simultaneous Turbulence and Ice Accretion on Small Fixed-Wing UAV Performance

T. Y. Ma*, N. Carlier, N. Kay†,
Department of Mechanical and Mechatronics Engineering, University of Auckland, Auckland, New Zealand

A. Pirooz,
National Institute of Water and Atmospheric Research, Auckland, New Zealand

C. Azorin-Molina
Spanish National Research Council (CIDE-CSIC), Valencia, Spain

ABSTRACT

Small Unmanned Aerial Vehicles (UAVs) are often required to operate in unfavourable weather conditions, such as unsteady turbulent winds and potentially in icing conditions. While the effects of turbulence and icing on small UAVs have been considered individually, little has been said of their combined effect on flight performance, endurance, and so the consequent probability of successfully completing the operation. As such, this work looks at the overall impact of simultaneous ice-accretion and turbulence conditions on aircraft performance for a fixed-wing Kahu UAV via wind tunnel testing. It was observed that ice has surprisingly little effect on the aerodynamic forces produced by the Kahu UAV, with one ice condition enhancing the lift-to-drag ratio. In contrast, increasing turbulence intensity significantly altered all forces and moments. The greatest change due to icing was seen in the roll moment variability. It is concluded that Kahu can be operated in icing conditions, albeit with a loss of endurance due to the excess power required.

1 INTRODUCTION

The utility of small UAVs has expanded rapidly, due to the development of small, lightweight electronics [1, 2]. Courtesy of their small size, these aircraft are able to operate in "dull, dirty and dangerous" environs which are either too hazardous for conventional aircraft, or not financially viable for the latter due to the supporting infrastructure required [3]. While multirotor configurations are favoured for short-range operations requiring hovering, fixed-wing designs, typically up to 2 m in span, offer range and endurance at low cost [4]. Although these may look like ordinary aircraft on a smaller scale, they differ aerodynamically through their much lower Reynolds numbers, often less than 250,000, and the consequent low-energy laminar boundary layer.

With regulations and roles often forcing small, UAVs to low altitudes, these aircraft are exposed to the highly unsteady flows seen low in the Atmospheric Boundary Layer (ABL). This combines with the typically-low flight speed of these aircraft to produce high onset turbulence intensities, reaching as high as 30% in urban operating conditions. The combination of low Reynolds number aerofoils has been found to result in significant unsteady flow separation, producing transient loads akin to dynamic stall. The mean lift coefficient at stall, however, can reduce by as much as 30%, while stall occurs at a higher Angle of Attack (AoA) [5]. This provides a significant challenge for UAV operations.

Icing is also a major challenge for research and rescue operations, when small UAVs are required to work in cold environments. As with turbulence, icing has a disproportionate effect on small UAVs due to their relatively low mass compared to the ice weight [6]. Aerodynamically, ice has a significant effect due to the sensitivity of the boundary layer at low Reynolds numbers. Hann and Johansen [6] noted that not only does stall occur at a lower AoA, with the loss of lift reaching 30%, but also drag doubles from the baseline value. Additionally, de-icing equipment is rarely fitted due to the limited mass and power capacity available onboard the aircraft [7].

In operation, a small UAV may encounter both turbulence and icing. While studies have been conducted for the individual effects of these environmental factors, the combination of the two has received little attention. Therefore, this work expands on the current knowledge base by looking at the impact of ice on the performance of a small UAV in turbulence.

2 PHYSICAL TESTING

The aircraft employed in this work is a fixed-wing Kahu UAV. This aircraft has been used for prior icing research, notably by Williams et al. [8]. It has a span of 2.316m, operating mass of 3.5 kg, and a cruising speed of 16.7 m s^{-1} (60 km/h). This results in a typical Reynolds number (based on the mean aerodynamic chord) around 230,000. The aircraft

* trista.ma@auckland.ac.nz
† nicholas.kay@auckland.ac.nz

can be seen in Figure 1 in the University of Auckland Boundary Layer Wind Tunnel.

Aerodynamic forces acting on the aircraft were recorded via a JR3 160M50A4-180-EF six-axis analogue loadcell for 60 seconds at a frequency of 1000 Hz. The data of interest were the lift, drag and pitch moments, as well as any changes in the roll moment. These have been presented as coefficients, as represented in Eqs. 1 to 4, for the lift (L), drag (D), pitch (M) and roll moments (R). Note the q is the dynamic pressure, S the reference wing area (0.484 m), c is the mean wing chord (0.209 m) and b is the wing span. Data was recorded in 2° Angle of Attack (AoA) increments from -10° to +20°, based on the wing root chordline. Force and moment offsets due to the stand were subtracted prior to analysis. With the test section 3.6 m wide and 2.5 m tall, the maximum blockage was 4%, and so velocity corrections were not applied.

Figure 1: Kahu UAV on load cell, with turbulence grid upstream

$$C_L = L/qS \quad (1)$$

$$C_D = D/qS \quad (2)$$

$$C_M = M/qSc \quad (3)$$

$$C_{Roll} = L/qSb \quad (4)$$

To simulate atmospheric turbulence, a passive, biplane turbulence grid was placed upstream of the aircraft as required, which can be seen in Figure 1. By varying the distance between the grid and Kahu, the turbulent flow conditions listed in Table 1 were produced. The primary parameter varied was the turbulence intensity. Although less than seen in an urban environment, this is still significant in the context of UAV operations. The use of this passive grid restricted the wind tunnel speed to 10 m s^{-1}, due to back pressure on the axial-flow fans. This resulted in an experimental mean-chord Reynolds number of 140,000. While less than ideal, the elevated turbulence intensity was anticipated to mitigate the difference in Reynolds number.

The ice shapes used in this work were those of Williams et al. [8]. These were generated on an RG-15 wing section (as used by Kahu) in an icing wind tunnel to the conditions of FAR Part 25 Appendix C. These represent cruising at an altitude of 1.5 km in an ambient -20°C, with a liquid water content of 1.9 g m^{-3}. Williams et al. [8] defined this as an "Intermittent Maximum" (IM) condition, and so each ice shape is designated by this and the AoA at which it was formed in Table 2. These profiles were extruded along the wing form of Kahu and 3D printed for wind tunnel testing. Ice on the tail unit and fuselage was not considered. The mass of each ice shape was determined from the CAD and added to the baseline net aircraft mass for performance assessment. This was conducted for each combination of ice shape and onset turbulence.

Turbulence Intensity, I_u	Length Scale, L_{xx}
1.1%	0.56 m
5.6%	0.32 m
8.0%	0.44 m
13.3%	0.42 m

Table 1: Turbulence Characteristics

State		**Aircraft Mass (kg)**	**Form**
No Ice		3.50	
Ice	0° IM	3.60	
	+4° IM	3.66	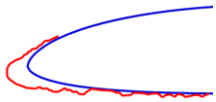
	-4° IM	3.66	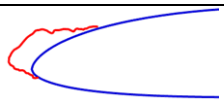

Table 2: Ice shapes and aircraft net mass

3 RESULTS

3.1 Time-Averaged Forces and Moments

Considering time-averaged data first, Figure 2 shows the clean Kahu airframe mean lift-to-drag ratio to be relatively insensitive to turbulence, maintaining a maximum C_L/C_D of 15.3, between 2° to 4° AoA for all turbulence intensities. While the addition of ice does not change the AoA of the maximum C_L/C_D, it does change the magnitude, as well as sensitivity to turbulence. This is best seen in the +4° IM and -4° IM cases. For the former, the maximum C_L/C_D increases to 16.3 at the lowest turbulence intensity, rising to 19.2 at the highest. This shape is seen in Table 2 to be the most conformal to the aerofoil geometry, and provides a small cambered leading edge extension. The -4° IM case, in contrast, lowers the maximum C_L/C_d to 13.2 when I_u = 1.1%, rising to C_L/C_d to 15.7 when I_u = 13.3%. This reduced aerodynamic performance can also be deduced from the form of the ice shape, which decambers the leading edge as a prominent upper-surface feature.

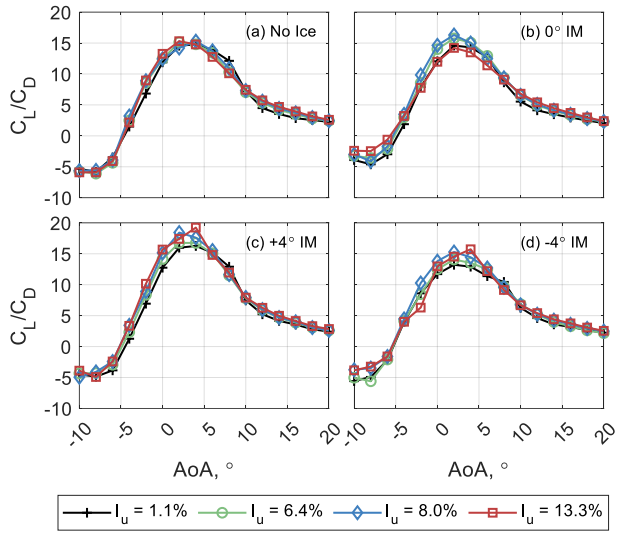

Figure 2: Time-averaged Lift-to-Drag Ratio for each ice configuration at all turbulence intensities.

Figures 3 and 4 resolve the lift and drag coefficients individually. The maximum lift coefficient for all cases can be seen in Figure 3 to initially rise with turbulence intensity, but reduces at the highest I_u as the lift slope declines. The AoA for maximum lift also increases with I_u. This is consistent with findings for reference aerofoils under similar conditions [5]. However, regardless of turbulence intensity, all ice shapes produce a more gradual stall than the baseline wing. This may be due to the ice shapes forcing an earlier boundary layer transition, and so delaying separation [9]. Oo et al. [10] observed aa laminar separation bubble for the Kahu wing in CFD with no onset turbulence, whereas ice promoted attached flow. This difference is mitigated at higher turbulence intensities, when laminar flow is unlikely to occur on the baseline wing [11].

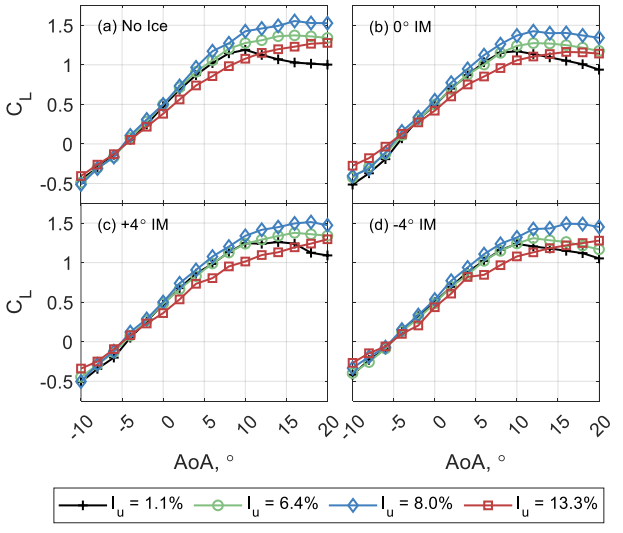

Figure 3: Time-averaged Lift Coefficient for each ice configuration at all turbulence intensities.

Unexpectedly, there is relatively little difference between the ice shapes and the clean wing, albeit with the +4° IM producing a slightly delayed stall. This is in contrast to the findings of Hann and Johansen [6] and Cheng et al. [12], who saw a reduction in the maximum lift coefficient exceeding 10%. The latter study, however, does not state the onset turbulence intensity. The baseline in the present work is 1.1%: this would be a significant factor in comparison to a smooth onset flow. Furthermore, Cheng et al. [12] use the effective wing area, including the change in reference planform due to the ice extending beyond the wing leading edge. Williams et al. [8] also note this as a factor for reducing the prominence of the ice, but also observe that it is impractical to change wing areas for different cases. In the present study, the ice would increase the wing area by 2.4%, 2.7% and 2.6% for the 0° IM, +4° IM and -4° IM, respectively.

Comparing to an experimental study with a similar baseline turbulence intensity, Oo et al. [10] recorded greater deviations in force due to the same ice shapes on the same wing. The difference, however, is that the aforementioned study looked solely at the wing and projected performance changes on the entire aircraft. The present work includes the entire airframe. Therefore, other sources of lift, notably the tailplane, are also included in the recorded data. This would dilute the impact of the ice, which is only applied to the wing.

As with the lift coefficient, Figure 4 shows that the primary difference in drag is evident around stall. While there is a slight reduction in drag at low AoA with increasing I_u, but an increase with ice, the overall form and magnitude are comparable. Above 10°, however, there is a significant increase in drag at the lowest turbulence intensity, the slope reducing again beyond 16°. As the turbulence intensity increases to 5.6% and 8.0%, this latter reduction in slope does not occur, the drag coefficient instead continuing to rise. This aligns with the findings of Tran et al. [13] for an isolated Kahu wing. On the other hand, at the highest turbulence intensity, the initial increase in drag is flattened out. The reason for this is not immediately clear, although this may be due to the delayed stall observed in the lift.

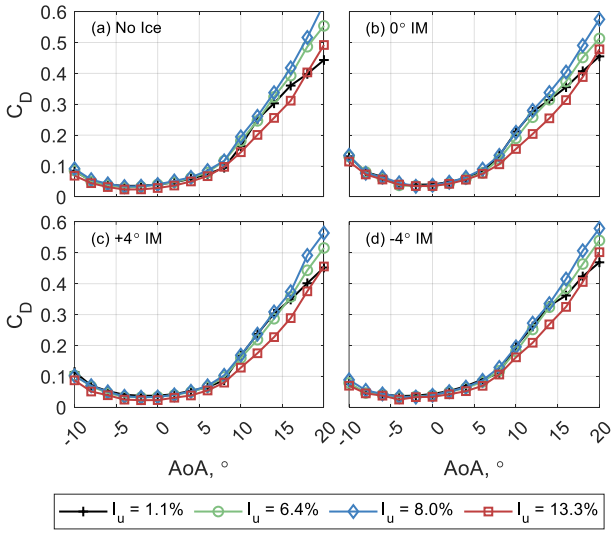

Figure 4: Time-averaged Drag Coefficient for each ice configuration at all turbulence intensities.

The moment coefficient, seen in Figure 5, displays more variability with ice, particularly at the highest turbulence intensity. Note that the high magnitude of the nose-down pitch moment at high AoA is due to the lift generated by the tailplane, cited 0.56 m aft of the CoG. The primary difference is the more nose-up moment of the 4° IM condition at AoA below 10°, which then becomes more negative than the baseline above this AoA at the lowest turbulence intensity. As the latter increases, a more nose-up moment is produced for all ice shapes. Given that the magnitude of the pitch moment coefficient remains within the bounds of what is seen with the clean wing, this indicates that Kahu would still have sufficient pitch authority in the absence of turbulence.

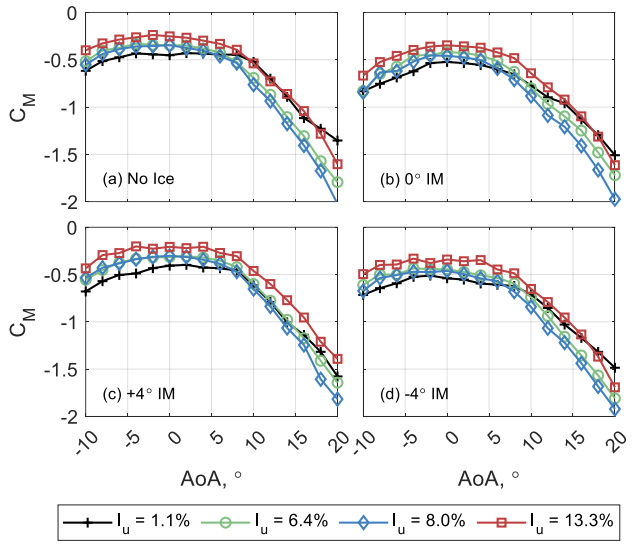

Figure 5: Time-averaged Pitch Moment Coefficient for each ice configuration at all turbulence intensities.

3.2 Unsteady Loads

Due to the highly unsteady onset flow, the resulting forces acting on the aircraft are also expected to be increasingly unsteady. The standard deviation is used to quantify this unsteadiness, and can be seen in Figures 6, 7, and 8 for the lift, drag and pitch moment coefficients, respectively. As with the time-averaged cases, the onset turbulence dominates the effect of the icing. This notably is seen primarily between $I_u = 1.1\%$ and $I_u = 5.6\%$, subsequent increases in turbulence intensity producing lesser changes in the unsteady loads. The magnitudes for the clean wing and all iced conditions are, in general, similar. Again, this is likely due to the effect of the rest of the airframe, with the tailplane providing a significant contribution to the pitch moment in particular.

Where differences can be seen is around stall. Whereas a sharp rise in unsteadiness can be seen for the iceless case, all iced conditions see a more gradual increase for each load. This may be due to promoting localised separation of the shaper leading edge earlier, leading to transient vortex shedding [14] and so greater force variability at a lower AoA. The 0° IM case also shows a notable increase in σ_{C_D} relative to other cases when $I_u = 15\%$. The reason for this is unclear: there is no corresponding increase in the standard deviation of the lift and pitch moment coefficients, which suggests it is not related to mass flow separation. Local separation has been noted to cause high-frequency unsteadiness in the pressure coefficient [15], but this has only been observed at low turbulence intensities. as with the laminar separation bubble, these effects would be unlikely to be evident as the onset flow becomes more unsteady and inhibits the maintenance of a laminar boundary layer.

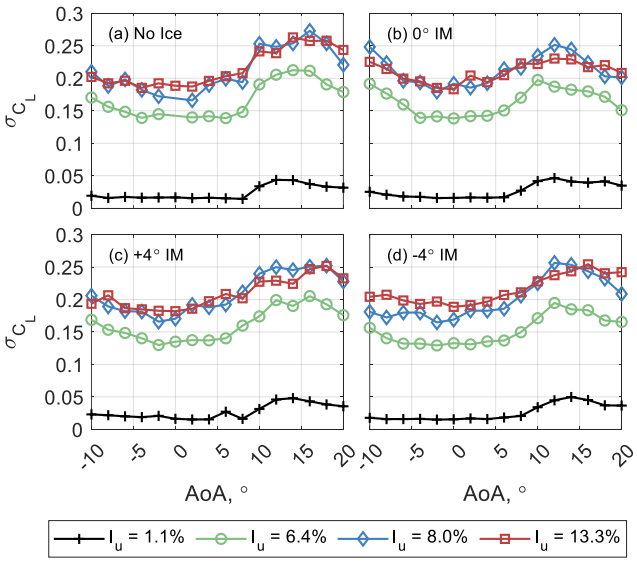

Figure 6: Standard deviation of the Lift Coefficient for each ice configuration at all turbulence intensities.

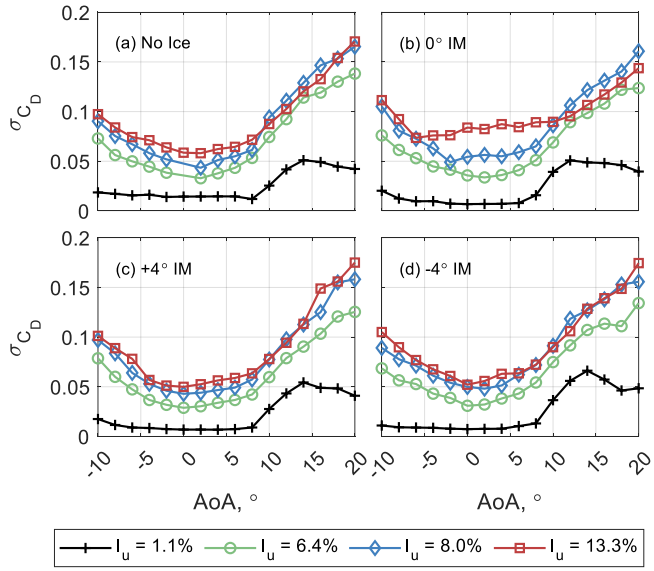

Figure 7: Standard deviation of the Drag Coefficient for each ice configuration at all turbulence intensities.

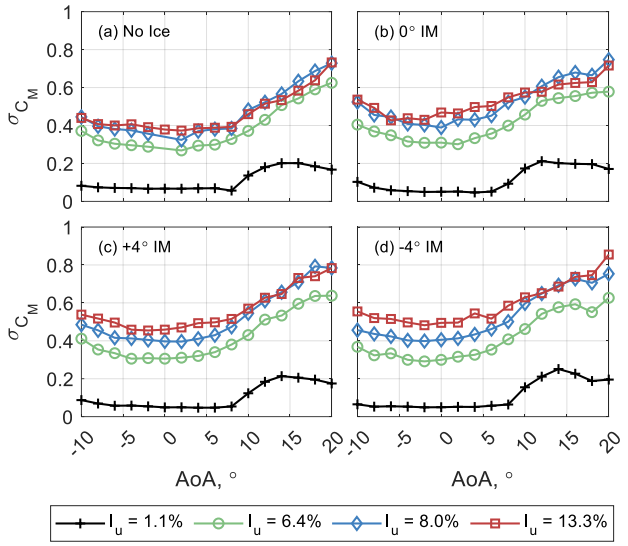

Figure 8: Standard deviation of the Pitch Moment Coefficient for each ice configuration at all turbulence intensities.

Additionally, the roll moment coefficient is presented in Figure 9. The time averaged mean was not shown as this is zero for all AoA (Kahu being restrained, symmetrical and oriented into the wind). However, Marino et al. [16] observed that roll deviation was the greatest concern for managing flightpath deviation and stable photography. At low flight speeds, the spanwise coherence of turbulent flow conditions is reduced, increasing susceptibility to roll disturbances [17].

As expected, increasing the turbulence intensity increases $\sigma_{C_{Roll}}$. Again, this is most prominent between the lower turbulence intensities, higher intensities producing little difference for the clean airframe. There is also an increase at stall, local vortex shedding occurring as the flow separates from the wing.

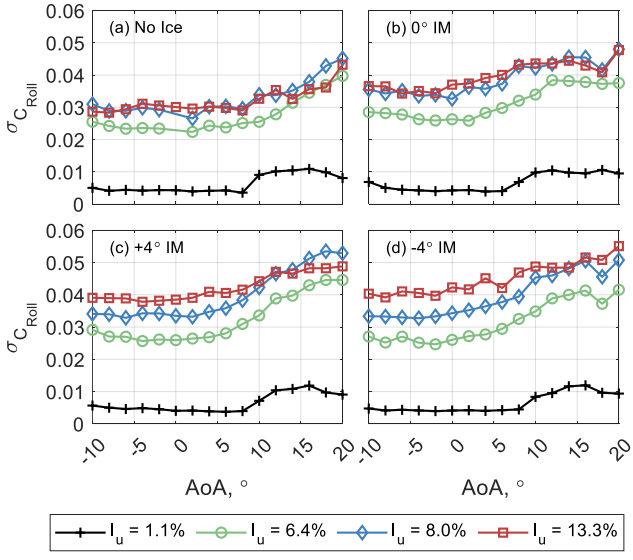

Figure 9: Standard deviation of the Roll Moment Coefficient for each ice configuration at all turbulence intensities.

However, the ice shapes do show a difference, generally inducing a higher roll moment variation at higher turbulence intensities for all AoA. This may be related to the ease of separation expected to be induced by the sharper leading edge [14]. Roll is more sensitive than the lift and drag coefficients in this regard due to the moment arm involved. As different flow conditions are seen along the span of the wing, local vortex formation and flow separation can occur simultaneously at different distances from the centre of gravity. For net forces, some of these local effects average out across the span. For a moment, however, this local variation can add together to produce a net increase. As such, the effect of the ice become more notable for roll, with its long offset to the centre of gravity. The pitch moment is less impacted due to the short moment arm of the wing in this axis.

3.3 Flight Performance

Two aspects are looked at for observing the impact of the ice and turbulence on overall flight performance: minimum flight speed and excess power required. The former can be seen in Table 3. Due to the unsteady nature of the forces generated, this speed is taken with the maximum 5th percentile lift. Use of the maximum time-averaged lift would result in significant periods of insufficient lift to fly, the wing intermittently stalling [5], while use of the minimum would be overly-conservative due to noise in the peak loads. As propulsive efficiency curves are not available, the vertical contribution of motor thrust is neglected, but would slightly decrease this speed.

I_u	No Ice	0° IM	+4° IM	-4° IM
1.1%	10.1	10.4	10.1	10.1
5.6%	10.6	11.0	10.7	11.0
8.0%	10.1	10.8	10.5	10.5
13.3%	11.4	12.1	11.4	11.6

Table 3: Minimum Flight Speed based on maximum 5th percentile lift, m s^{-1}

The presence of ice has minimal impact on the minimum speed. While this is surprising, given the extra mass due to the ice, the increase in the lift generated at higher AoA offsets this. In contrast, increasing the onset turbulence intensity increases the flight speed required, primarily due to the increasing spread of lift coefficients produced. This is most apparent at the highest turbulence intensity, where not only is the spread of transient lift greater, but also the maximum mean lift coefficient produced has reduced.

The excess power required can be seen in Table 4. This is the power difference from the baseline case to maintain flight with best endurance as the target. As such, the minimum power required was calculated for each mass and set of aerodynamic data, and the difference found from the baseline. With the exception of +4° IM at the lowest turbulence intensity, any ice or increase in turbulence intensity produces a greater power requirement. This is again

dominated by turbulence, reflecting the greater power needed to maintain safe flight. The increase in power for the ice primarily comes from the greater AoA needed to offset the weight, and as a consequence an increase in drag. The +4° IM case has the benefit of its mild increase on both area and camber producing a higher lift-to-drag ratio.

I_u	No Ice	0° IM	+4° IM	-4° IM
1.1%	0.00	2.94	0.00	6.65
5.6%	11.22	15.54	11.75	18.29
8.0%	12.26	20.35	13.24	19.02
13.3%	36.47	48.13	28.72	30.56

Table 4: Excess power required at minimum power velocity, W

With a 1.2 kW motor, it is unlikely that that Kahu would be unsafe to operate in such conditions, and overall Kahu seems to be more resilient to icing than expected. However, these power increases would result in a loss of endurance. Previous work found that Kahu typically consumes around 100 W [18] in flight with all systems operational. Taking this value, the endurance loss in the highest turbulence intensity with the 0° IM ice shape would be as much as 48%. Flying slightly nose-up into adverse conditions, as per the +4° IM case mitigates this.

4 DISCUSSION

The present work looked only at wing icing due to the icing data available. However, ice is also known to significantly impact propeller aerodynamics. This would reduce power output, and hence the margin available to offset the added power requirements due to ice and turbulence.

The impact of tailplane icing has also not been considered. It is unclear how much ice would form on the tailplane, sited in the wake of the propeller. Scaling the ice shapes used here to the tailplane geometry produces a net added mass of 7.9 g, or a nose-up moment of 4.7 Nm when flying with a horizontal attitude (maximum moment arm). In terms of the pitch moment in Figure 5, this would be a negligible change in C_M of 7.5×10^{-4}. However, the impact on airframe drag or on tailplane control authority cannot be estimated in such a manner. Kahu has an all-moving tail unit: the effects of ice on the wing would suggest that sufficient AoA range would remain available for control to be effective. To obtain a better picture, ice should be generated on the whole Kahu airframe with a variety of power settings and tailplane rotations.

The impact of icing on control surface effectiveness was also not considered, as the wind tunnel model does not have operable control surfaces. It would be of interest to assess the changes in effectiveness of each surface in the presence of the upstream disturbances.

Finally, a major constraint in wind tunnel testing with turbulence is the inability of the UAV to move with the flow. In reality, the aircraft does not see the full gust variability as it is displaced by the gust. This can result in overestimation of peak loads, and so a conservative decision on whether it is safe to fly. While this is better than the converse situation, it does remain a limitation on the applicability of the wind tunnel data.

4. CONCLUSIONS

While both icing and turbulence impact the aerodynamic performance of the Kahu UAV, generally the effect of turbulence dominates that of the ice. The primary instance when the impact of ice is evident is towards stall. Surprisingly, one of the icing conditions improved the lift to drag ratio, likely through suppression of laminar separation in addition to increasing the effective wing area and camber. Thus, the effects of icing and turbulence are minimised if the UAV is flown into icing conditions with a slight nose-up attitude. Due to the propulsive power available on Kahu, it is unlikely that cancellation of the flight would be necessary, although the endurance would be decreased.

ACKNOWLEDGEMENTS

This research was conducted as a Final Year Research Project (BE(Hons)) in the Boundary Layer Wind Tunnel at the University of Auckland.

This study forms part of the ThinkInAzul programme and was supported by MCIN with funding from European Union NextGenerationEU (PRTR-C17.I1) and by Generalitat Valenciana (THINKINAZUL/2021/018).

REFERENCES

[1] S. Aggarwal and N. Kumar, "Path planning techniques for unmanned aerial vehicles: A review, solutions, and challenges," *Computer communications,* vol. 149, pp. 270-299, 2020.

[2] J. M. McMichael and M. S. Francis, "Micro air vehicles-toward a new dimension in flight," DARPA, USA, 1997.

[3] R. Austin, *Unmanned aircraft systems: UAVS design, development, and deployment*, 1 ed. (no. Book, Whole). West Sussex, UK: John Wiley & Sons, 2010.

[4] P. Fahlstrom and T. Gleason, *Introduction to UAV Systems*, 4 ed. (Introduction to UAV systems, no. Book, Whole). West Sussex, UK: John Wiley & Sons, 2012, pp. 17-31.

[5] N. J. Kay, P. J. Richards, and R. N. Sharma, "Influence of Turbulence on Cambered and Symmetrical Airfoils at Low Reynolds Numbers," *AIAA Journal,* vol. 58, no. 5, pp. 1913-2325, 2020, doi: https://doi.org/10.2514/1.J058822.

[6] R. Hann and T. A. Johansen, "UAV icing: The influence of airspeed and chord length on performance degradation," *Aircraft Engineering and Aerospace Technology,* vol. 93, no. 5, pp. 832-841, 2021.

[7] L. Zhou, X. Yi, and Q. Liu, "A Review of Icing Research and Development of Icing Mitigation Techniques for Fixed-Wing UAVs," *Drones,* vol. 7, no. 12, p. 709, 2023.

[8] N. Williams, A. Benmeddour, G. Brian, and M. Ol, "The effect of icing on small unmanned aircraft low Reynolds number airfoils," in *17th Australian International Aerospace Congress: AIAC 2017*, 2017, no. Conference Proceedings: Engineers Australia, Royal Aeronautical Society, p. 19.

[9] M. Istvan, J. Kurelek, and S. Yarusevych, "Effects of free-stream turbulence intensity on laminar separation bubbles," in *46th AIAA Fluid Dynamics Conference*, Washington D.C., USA, 2016, no. Conference Proceedings: AIAA, pp. 1-13, doi: https://doi.org/10.2514/6.2016-3946. [Online]. Available: https://www.scopus.com/inward/record.uri?eid=2-s2.0-84980410219&partnerID=40&md5=c2da9bd9b85ffd99783396218b437394

[10] N. L. Oo, N. J. Kay, A. J. Brenkley, and R. N. Sharma, "Investigation into the behaviour of an iced low Reynolds number aerofoil," in *10th International Micro-Air Vehicles Conference*, Melbourne, VIC, Australia, Ruasrt, Ed., 2018 2018, no. Conference Proceedings: IMAV, pp. 174-179. [Online]. Available: http://www.imavs.org/papers/2018/IMAV_2018_paper_5.pdf. [Online]. Available: http://www.imavs.org/papers/2018/IMAV_2018_paper_5.pdf

[11] T. J. Mueller, L. J. Pohlen, P. E. Conigliaro, and B. J. Jansen Jr, "The influence of free-stream disturbances on low Reynolds number airfoil experiments," *Experiments in Fluids,* vol. 1, no. 1, pp. 3-14, 1983, doi: https://doi.org/10.1007/BF00282261.

[12] H. Cheng, D. Zhao, N. L. Oo, X. Liu, and X. Dong, "Numerical Investigation on Intermittent Maximum Ice Accretion and Aerodynamic Performances of RG-15 Aerofoil at Low Reynolds Number," *Aerospace,* vol. 11, no. 1, p. 7, 2023.

[13] H. B. N. B. Tran, P. J. Richards, and R. N. Sharma, "Unsteady Aerodynamic Response of the Kahu UAV Wing under Turbulent Conditions," in *AIAA AVIATION 2021 FORUM*, 2021, p. 2582.

[14] J. H. S. Fincham and M. I. Friswell, "Aerodynamic optimisation of a camber morphing aerofoil," *Aerospace Science and technology,* vol. 43, pp. 245-255, 2015, doi: https://doi.org/10.1016/j.ast.2015.02.023.

[15] N. L. Oo, P. J. Richards, and R. N. Sharma, "Ice-Induced Separation Bubble on RG-15 Airfoil at Low Reynolds Number," *AIAA Journal,* vol. 0, no. 0, pp. 1-12, doi: 10.2514/1.J059257.

[16] M. Marino, S. Watkins, R. Sabatini, and A. Gardi, "Unsteady pressure measurements on a MAV wing for the design of a turbulence mitigation system," in *Metrology for Aerospace (MetroAeroSpace)*, 2014 2014, no. Conference Proceedings: IEEE, pp. 138-143, doi: https://doi.org/10.1109/metroaerospace.2014.6865909.

[17] S. Watkins, J. Milbank, B. J. Loxton, and W. H. Melbourne, "Atmospheric winds and their implications for Micro Air Vehicles," *AIAA Journal,* vol. 44, no. 11, pp. 2591-2600, 2006, doi: https://doi.org/10.2514/1.22670.

[18] A. Gong, J. L. Palmer, G. Brian, J. R. Harvey, and D. Verstraete, "Hardware-in-the-loop simulation of a fuel-cell-based UAV propulsion system using real-world flight data," in *Proceedings of the Fourth Australasian Unmanned Systems Conference, Australian Association for Unmanned Systems*, 2014, p. 7.